

DEPARTMENT OF ELECTRICAL AND COMPUTER ENGINEERING
COLLEGE OF ENGINEERING AND TECHNOLOGY
OLD DOMINION UNIVERSITY
NORFOLK, VIRGINIA 23529

IN-61-CP
2612
p-61

**A NEW METHOD FOR RECOGNIZING QUADRIC SURFACES FROM RANGE DATA
AND ITS APPLICATION TO TELEROBOTICS AND AUTOMATION (FINAL PHASE)**

By

Roland Mielke, Principal Investigator

Ivan D' Cunha, Research Associate

Nicolas Alvertos, Research Associate

Final Report
For the period ended February 28, 1994

N94-28825

Unclas

G3/61 0002612

Prepared for
National Aeronautics and Space Administration
Langley Research Center
Hampton, Virginia 23665

Under
Master Contract NAG-1-1223
Plesent W. Goode IV, Technical Monitor
ISD-Automation Technology Branch

March 1994

(NASA-CR-195733) A NEW METHOD FOR
RECOGNIZING QUADRIC SURFACES FROM
RANGE DATA AND ITS APPLICATION TO
TELEROBOTICS AND AUTOMATION, FINAL
PHASE Final Report, period ending
28 Feb. 1994 (Old Dominion Univ.)
61 p

DEPARTMENT OF ELECTRICAL AND COMPUTER ENGINEERING
COLLEGE OF ENGINEERING AND TECHNOLOGY
OLD DOMINION UNIVERSITY
NORFOLK, VIRGINIA 23529

**A NEW METHOD FOR RECOGNIZING QUADRIC SURFACES FROM RANGE DATA
AND ITS APPLICATION TO TELEROBOTICS AND AUTOMATION (FINAL PHASE)**

By

Roland Mielke, Principal Investigator

Ivan D' Cunha, Research Associate

Nicolas Alvertos, Research Associate

Final Report

For the period ended February 28, 1994

Prepared for
National Aeronautics and Space Administration
Langley Research Center
Hampton, Virginia 23665

Under
Master Contract NAG-1-1223
Plesent W. Goode IV, Technical Monitor
ISD-Automation Technology Branch



March 1994

**A New Method for Recognizing Quadric Surfaces from Range Data and
Its Application to Telerobotics and Automation
(final phase)**

by

Nicolas Alvertos*, Ivan D'Cunha**, and Roland Mielke***

Abstract

In the final phase of the proposed research a complete top to down three dimensional object recognition scheme has been proposed. The various three dimensional objects included spheres, cones, cylinders, ellipsoids, paraboloids, and hyperboloids. Utilizing a newly developed blob determination technique, a given range scene with several non-cluttered quadric surfaces is segmented. Next, using the earlier (phase 1) developed alignment scheme, each of the segmented objects are then aligned in a desired coordinate system. For each of the quadric surfaces based upon their intersections with certain pre-determined planes, a set of distinct features (curves) are obtained. A database with entities such as the equations of the planes and angular bounds of these planes has been created for each of the quadric surfaces. Real range data of spheres, cones, cylinders, and parallelepipeds have been utilized for the recognition process. The developed algorithm gave excellent results for the real data as well as for several sets of simulated range data.

* Adjunct Faculty, Department of Electrical and Computer Engineering,
Old Dominion University, Norfolk, Virginia 23529-0246.

** Graduate Research Assistant, Department of Electrical and Computer Engineering,
Old Dominion University, Norfolk, Virginia 23529-0246.

*** Chairman, Department of Electrical and Computer Engineering,
Old Dominion University, Norfolk, Virginia 23529-0246.

1. INTRODUCTION

One of the most important tasks in computer vision is that of three-dimensional object recognition. Unlike the recognition procedure developed for intensity-based images, the recent development of active and passive sensors extracting quality range information has led to the involvement of explicit geometric representations of the objects for the recognition schemes [1,2]. Location and description of three-dimensional objects from natural light images are often difficult to determine. However, range images give a more detailed and direct geometric description of the shape of the three-dimensional object.

The laser range-finder makes use of a laser beam which scans the surfaces in the scene of observation from left to right and top to bottom. Thus the distances obtained measure both depth and scanning angle. The principle of triangulation is often utilized to obtain the three-dimensional coordinate of each pixel. Unless a specific algorithm demands a special form of the range images, it is usually this depth information which is utilized for the recognition process. Active triangulation techniques use an extra source of light to project some pattern onto the objects to be measured, thereby reducing complexity of the stereo matching problem [3,4]. Many industrial and navigational robotic tasks such as target identification and tracking, automated assembly, bin picking, mobile robots, etc., will be better accomplished if such explicit depth information can be efficiently obtained and accurately interpreted.

1.1 Objectives and Organization of the Report

An approach based on two-dimensional analytic geometry to recognize a series of three-dimensional surfaces is presented in this research. Among the various three-dimensional surfaces considered are the hyperboloids of one and two sheets, ellipsoids, spheres, circular and elliptical quadric cones, circular and elliptical cylinders, parabolic and hyperbolic cylinders, elliptic and hyperbolic paraboloids, and parallelepipeds.

The difficulties in recognizing three-dimensional surfaces stems from the complexity of the scene, the number of surfaces in the database and the lack of *a priori* information about the scene. Techniques vary based upon the difficulty of the recognition problem. In our case we attempt to recognize segmented surfaces in range images.

Location and orientation of three-dimensional surfaces has always been the most complex issue in many computer vision applications. Algorithms for a robust three-dimensional recognition system must be view-independent. Herein, we have developed a new technique to determine the three-dimensional surface location and orientation in range images. We consider objects which are composed of common quadric surfaces such as the ones described earlier. With this iterative technique the rotation parameters (product terms) of the general description of a quadric surface are eliminated, thus, aligning the surfaces with a common coordinate system. Convergence is achieved in less than seven iterations. Once the object lies in a desired stable rest position, it is intersected by a sufficient and necessary number of planes with different orientation so that an unique set of curves characterizing the surface is obtained. This minimum number of such planes can be estimated utilizing the analysis presented in this research, where angular (orientation) bounds within which any plane intersecting a surface results into the same type of curve are determined. In comparison to most of the present day methods applied for range image object recognition, the proposed approach attacks the problem in a different manner and is computationally inexpensive. This new work on surface recognition, combined with existing segmentation methodologies, could lead to the creation of a complete recognition scheme.

Section 2 reviews some of the earlier and current work in this area. Section 3 describes in detail newly developed techniques for range image edge detection and range image segmentation. In sections 4 and 5 we discuss, in detail, our proposed

three-dimensional approach. Results are summarized in Section 6. Six different sets of real range images of spheres, cylinders, and cones were utilized to test the proposed recognition scheme. Results obtained for simulated data of other quadric surfaces, namely, hyperboloids and paraboloids are also tabulated in Section 6. Section 7 concludes with a discussion of possible areas for future investigation.

2. BACKGROUND

Many of the currently available techniques for describing and recognizing three-dimensional objects are based on the principle of segmentation. Segmentation is the process in which range data is divided into smaller regions (mostly squares). These small regions are approximated as planar surfaces or curved surfaces based upon the surface mean and Gaussian curvatures. Regions sharing similar curvatures are subsequently merged. This process is known as region growing. Other approaches [4-10] characterize the surface shapes while dealing with the three-dimensional recognition problem. Levine et al. [11] briefly review various works in the field of segmentation, where segmentation has been classified into region-based and edge-based approaches. Again surface curvatures play an important role for characterization in each of these approaches.

Grimson et al. [12] discuss a scheme utilizing local measurements of three-dimensional positions and surface normals to identify and locate objects from a known set. Objects are modeled as polyhedra with a set number of degrees of freedom with respect to the sensors. The authors claim a low computational cost for their algorithm. Although they have limited the experiments to one model, i.e., data obtained from one object, they claim that the algorithm can be used for multiple object models. Also, only polyhedral objects with a sufficient number of planar surfaces can be used in their scheme.

Another paper by Faugeras et al. [13] describes surfaces by curves and patches which are further represented using linear parameters such as points, lines and planes. Their algorithm initially reconstructs objects from range data and consequently utilizes certain constraints of rigidity to recognize objects while positioning. They arrive at the conclusion that for an object to be recognized, at least a certain area of the object should be visible (approx. 50%). They claim their approach could be used for images obtained using ultrasound, stereo, and tactile sensors.

Hu and Stockman [14] have employed structured light as a technique for three-dimensional surface recognition. The objects are illuminated using a controlled light source of a regular pattern, thereby creating artificial features on the surfaces which are consequently extracted. They claim to have solved the problem known as "grid line identification." From the general constraints, a set of geometric and topological rules are obtained which are effectively utilized in the computation of grid labels which are further used for finding three-dimensional surface solutions. Their results infer that consistent surface solutions are obtained very fast with good accuracy using a single image.

Recognition of polyhedral objects involves the projection of several invariant features of three-dimensional bodies onto two-dimensional planes [15]. Recently, recognition of three-dimensional objects based upon their representation as a linear combination of two-dimensional images has been investigated [16]. Transformations such as rotation and translation have been considered for three-dimensional objects in terms of the linear combination of a series of two-dimensional views of the objects. Instead of using transformations in three-dimensions, it has been shown that the process is the equivalent of obtaining two-dimensional transformations of several two-dimensional images of the objects and combining them together to obtain the three-dimensional transformation. This procedure appears computationally intensive.

Most of the techniques and algorithms mentioned above have a common criterion for classifying the three-dimensional objects in the final phase. They have a database of all the objects they are trying to recognize and hence try to match features from the test samples to the features of the objects in the database.

Fan et al. [17] use graph theory for decomposing segmentations into subgroups corresponding to different objects. Matching of the test objects with the objects in the database is performed in three steps: the screener, which makes an initial guess for

each object; the graph matcher, which conducts an exhaustive comparison between potential matching graphs and computes three-dimensional transformation between them; and finally, the analyzer, which based upon the results from the earlier two modules conducts a split and merge of the object graphs. The distinguishing aspect of this scheme is that the authors used occluded objects for describing their proposed method.

Forsyth et al. [18] use stereo images to obtain a range of invariant descriptors in three-dimensional model-based vision. Initially, they demonstrate a model-based vision system that recognizes curved plane objects irrespective of the pose. Based upon image data, models are constructed for each object and the pose is computed. However, they mainly describe three-dimensional objects with planar faces.

Lee and Hahn [19] have actually dealt with an optimal sensing strategy. Their main objective is to obtain valuable and effective data or information from three-dimensional objects, which subsequently could be used to describe and recognize natural quadric surfaces. Works on stereo vision can be found in references 20, 21, 22 and 23.

3. RANGE IMAGE SEGMENTATION

A robust segmentation scheme is one of the primary requirements for three-dimensional object recognition. Partitioning a given image into homogeneous regions-this task has been the centerpiece of investigations of several major researchers all of these years.

In this research we propose a simplistic segmentation scheme for un-occluded cluttered three-dimensional objects in a scene. A assumption relating to the three-dimensional objects being quadric in nature, would further enable us demonstrate an object recognition scheme proposed in an earlier paper.

The proposed method involves the extraction of jump edges which we refer to as global edges. After having median filtered the resultant image thereby eliminating some of the spurious edges, a thinning algorithm is implemented which facilitates the utilization of a blob determination algorithm thereby completing the segmentation process. The blob finding algorithm which has been published earlier [30], the various objects in a scene are marked, each area representing a particular surface. Using few basic image processing techniques, such as image addition, subtraction, etc., each marked area is further mapped into a data file, which is further utilized to determine whether a given surfaces is quadric or some other surface.

3.1. Background

Most of the present day Segmentation techniques are classified as either region-based approach or edge based approach [11]. While in a region-based approach an image is segmented into regions corresponding to surface primitives which are further defined using analytical functions, an edge-based approach looks into

discontinuity in range images in both the surface as well as the surface orientation. Many of the segmentation techniques, both region-based and edge-based have been reviewed in detail by Levine et. al [11].

Aggarwal et al. [28] proposed a segmentation technique of Range images using pyramidal Data Structures. This approach consists of two levels of segmentations, a lower-level, which groups pixels based on local properties irrespective of the surface type, the higher-level segmentation is a surface based representation which groups pixels into homogeneous regions. Since local surface operations are involved, we consider this technique to be very computationally intensive.

3.2. Segmentation Scheme

As in the case of most segmentation based recognition schemes, our proposed technique has the following hierarchial outlook:

1. Edge marking,
2. Median filtering,
3. Image Thinning,
4. Contour filling,
5. Blob determination,
6. Image Data Mapping, and
7. Classification of the object as a quadric or non-quadric surface.

Since procedures 1 through 4 are well defined image processing routines, apart from a brief discussion about them, the succeeding part of the report will mainly concentrate from procedures 5 onwards.

Since three-dimensional range images are in question, edge-based approaches have been utilized. As mentioned earlier, objects in the image being cluttered but not occluded, we are only concerned about jump edges. After computing the difference in depth values, and using a suitable threshold, edges are marked on the real images. Subtracting these edge-marked images from the original range images yields the image of edges in the scene.

The classical thinning algorithm [29] is then implemented, whereby most of the edges are thinned to a pixel thickness. Since specks of isolated pixels and small

streaks of lines may result in some cases, a median filter eliminates most of these abnormalities to a large extent. Places where edges are prominent but have one or two pixels missing are filled using a contour filling algorithm proposed in [29]. At this instant the thinned-edge marked images are ready to undergo the blob or area determination routine. The procedure is explained next in detail.

The $N \times M$ image array is augmented by two columns (one to the left and one to the right) and two rows (one to the top and the other to the bottom) all filled with white pixels.

The white pixels of the first row are assigned an arbitrary value v . Beginning with the second row, whenever a white pixel is encountered the minimum assigned value of the two neighboring pixels, as shown in Figure 1a, is assigned to this pixel. All the black pixels encountered are assigned the value $NM + v$, where NM is the total number of all the pixels (black and white) in the character array and v is the initial value assigned to the white pixels of the first row. This value of $NM + v$ never changes. Whenever a white pixel has two neighboring black pixels as in Figure 1b, the value of v is incremented and the new value is assigned to this white pixel. The second step of the process involves the reassignment of all the white pixels with the minimum assigned value of the four neighboring sites as shown in Figure 1b. The assignment remains the same ($NM + v$) for black pixels. Step 2 is repeated for N (the number of rows) iterations. In step 3, the number of distinct integers other than v and $NM + v$ (assigned to black pixels) are detected as the number of levels L . The value of L then denotes the number of closed areas in a image.

This procedure can be summarized as follows. Let the pixels of the image array be denoted as

$$p(i,j), 1 \leq i \leq N + 2, 1 \leq j \leq M + 2,$$

$p(i,j) = 0$ refers a white pixel and

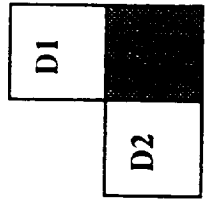


Figure 1a

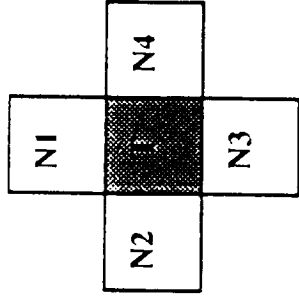


Figure 1b

Figure 1a. Minimum assigned value of D1 and D2 (D1 and D2 can be both white pixels or one white and the other black pixel) is assigned to T.

Figure 1b. The v of the T pixel is replaced with the minimum assigned v of N1, N2, N3, N4, and T.

$p(i,j) = 1$ refers a black pixel.

For all

$p(1,j), 1 \leq j \leq M + 2$

$p(N+2,j), 1 \leq j \leq M + 2,$

$p(i,1), 1 \leq i \leq N + 2,$

and

$p(i,M+2), 1 \leq i \leq N + 2,$ we assign the value $n_{i,j} = v.$

Beginning from the second row,

For $2 \leq i \leq N + 1, 2 \leq j \leq M + 1$

If $p(i,j) = 1,$ assign $n_{i,j} = NM + v$

If $p(i,j) = 0,$ then

if $p(i - 1,j) = p(i,j - 1) = 1,$ then $n_{i,j} = \max(n_{l,k}) + 1,$

for all $l \leq i, k < j,$ where $n_{l,k} \neq NM + v$

otherwise assign $n_{i,j} = \min(n_{i-1,j}, n_{i,j-1})$

During the second step, for

$2 \leq i \leq N + 1, 2 \leq j \leq M + 1,$

for each pixel $p(i,j),$ with assignment $n_{i,j} \neq NM + v$

assign $n_{i,j} = \min(n_{i-1,j}, n_{i,j}, n_{i,j-1}, n_{i,j+1}, n_{i+1,j})$

Step 2 is repeated N times.

In the third step,

initialize $L(\text{level}) = 1$

initialize maximum = 0

initialize minimum = $NM + v$

For all $2 \leq i \leq N + 1, 2 \leq j \leq M + 1,$

For all $n_{i,j} \neq NM + v,$ and $n_{i,j} \neq v,$

Find maximum and minimum of $n_{i,j},$

If maximum = zero, then,

Stop. The number of enclosed areas is Zero.

If maximum = minimum (\neq zero), then,

Stop. The number of enclosed areas is $L.$

Else,

(when maximum \neq minimum), then,

$$\text{Level}(L) = L + 1 .$$

Now for all $n_{i,j}$.EQ. minimum ,

assign , $n_{i,j} = \text{maximum}$.

re-initialize, minimum = maximum, and continue.

At the end of the loop the value of "L" gives the number of closed areas in a image. Each area is further marked an distint integer so as to map the particular range values to different data files.

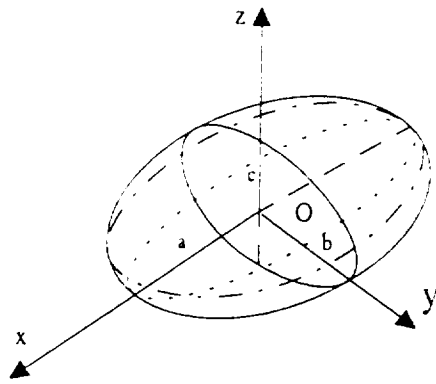
The experimental section consists of a particular image of a printed circuit board, wherein some of the objects have been classified as spheres, ellipses, and planar surfaces. Now that the surfaces have been segemented, in the next section we describe the recognition scheme in detail to recognize all of the quadric surfaces.

4. FORMULATION OF THE RECOGNITION SCHEME

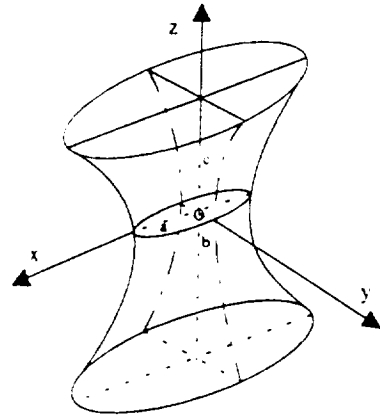
Figures 2, 3, and 4 illustrate the following three-dimensional quadric surfaces which are considered for the recognition process: ellipsoids, the hyperboloids of one and two sheets, quadric cones, elliptic paraboloids, hyperbolic paraboloids, elliptic cylinders, parabolic cylinders, hyperbolic cylinders, and parallelepipeds.

Most three-dimensional objects of practical use which are usually man-made, may be assumed to consist of at least one of the surfaces described above. All the representations of surfaces which were described above hold true under ideal conditions, i.e., when the source data is perfect, exact pose and orientation of the objects are known, the system is noiseless, etc. However in the real world, practically none of these conditions hold true. Any set of data, whether it is derived or generated from a passive (camera) or an active sensor (laser range mapper), can at best be approximated to a second-degree polynomial. Whether this polynomial accurately represents a surface or not, and if so, how these coefficients (representation) can be chosen to come close to recognizing a three-dimensional object, is the whole issue of the recognition problem.

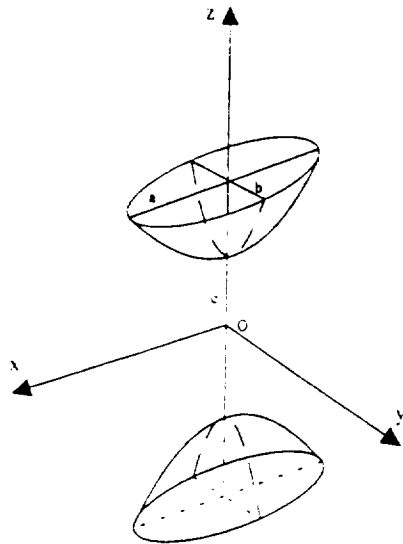
However, before elaborating on the recognition scheme, an overview of the technique is presented. The recognition scheme utilizes a two-dimensional discriminant (which is a measure for distinguishing two-dimensional curves) to recognize three-dimensional surfaces. Instead of utilizing the ten generated coefficients and attempting to recognize the surface from its quadric representation, the quadrics are identified using the information resulting from the intersection of the surface with different planes. If the surface is one of those listed above, there are five possible two-dimensional curves that may result from such intersections, (i) a circle, (ii) an ellipse, (iii) a parabola, (iv) a hyperbola, and (v) a line. Thus, a feature or pattern vector with five independent components can be formed for characterizing each of the surfaces.



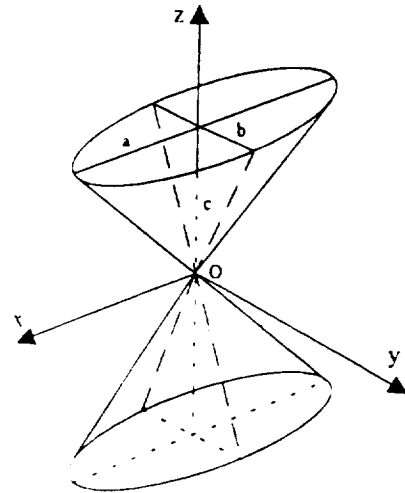
Real Ellipsoid: $\frac{x^2}{a^2} + \frac{y^2}{b^2} + \frac{z^2}{c^2} = 1$



Hyperboloid of one sheet: $\frac{x^2}{a^2} + \frac{y^2}{b^2} - \frac{z^2}{c^2} = -1$

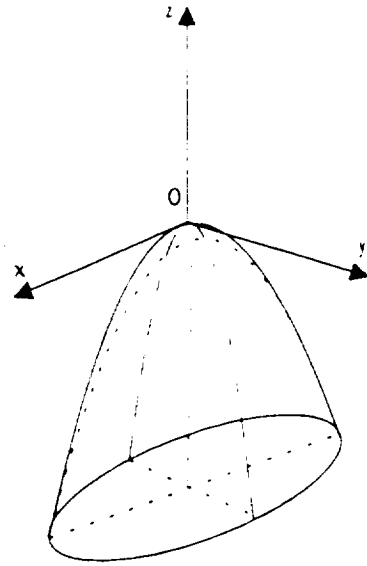


Hyperboloid of two sheets: $\frac{x^2}{a^2} + \frac{y^2}{b^2} - \frac{z^2}{c^2} = -1$

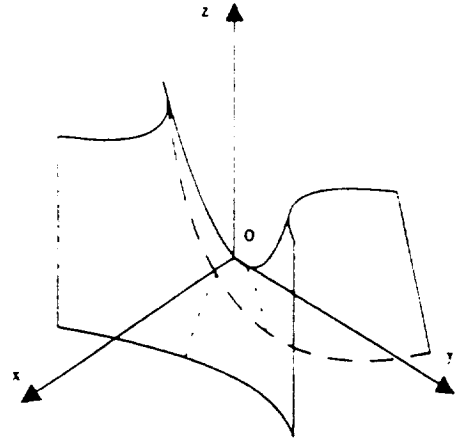


Real quadric cone: $\frac{x^2}{a^2} + \frac{y^2}{b^2} - \frac{z^2}{c^2} = 0$

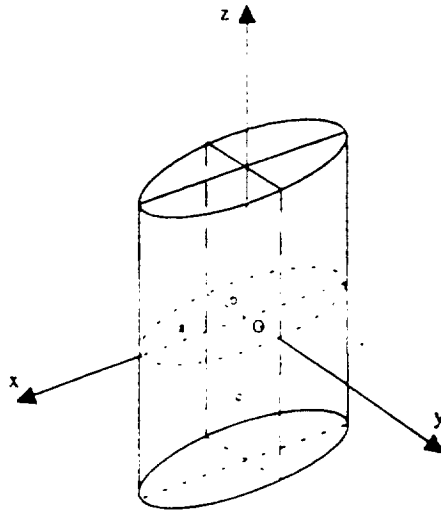
Figure 2. Quadric representations of Real ellipsoid. Hyperboloid of one sheet, Hyperboloid of two sheets, and real quadric cone.



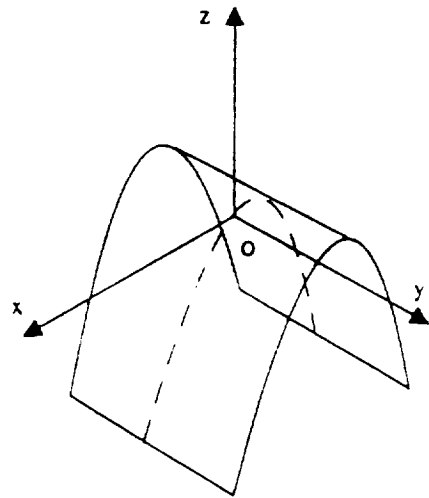
Elliptic paraboloid: $\frac{x^2}{a^2} + \frac{y^2}{b^2} + 2z = 0$



Hyperbolic paraboloid: $\frac{x^2}{a^2} - \frac{y^2}{b^2} + 2z = 0$

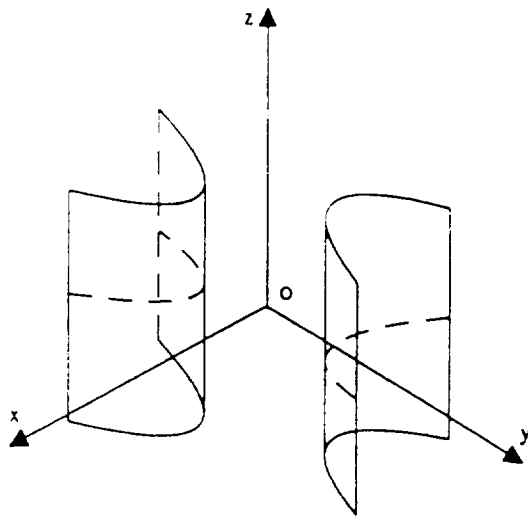


Elliptic cylinder: $\frac{x^2}{a^2} + \frac{y^2}{b^2} = 1$

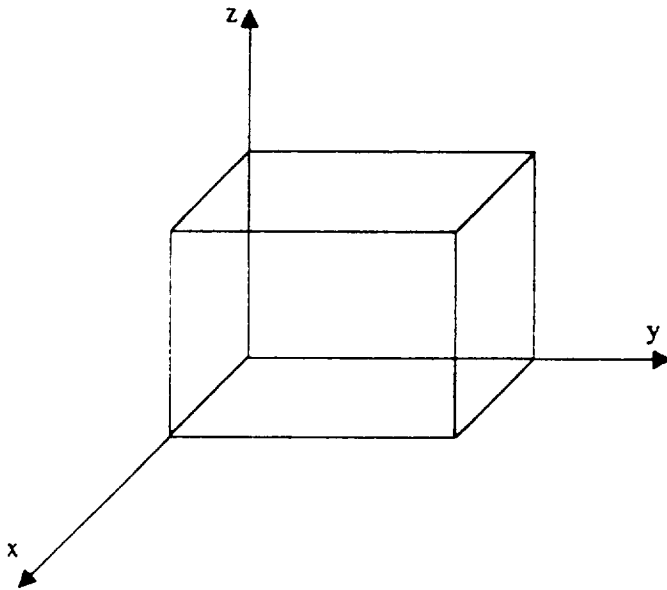


Parabolic cylinder: $x^2 + 2rz = 0$

Figure 3. Quadric representations of Elliptic paraboloid, Hyperbolic paraboloid, Elliptic cylinder, and Parabolic cylinder.



Hyperbolic cylinder: $\frac{x}{a^2} - \frac{y^2}{b^2} = -1$



Parallelepiped

Figure 4. Quadric representations of Hyperbolic cylinder and Parallelepiped.

4.1 Recognition Scheme

Our recognition scheme consists of the following steps:

- (1) acquisition of the range data and conducting the pre-processing steps,
- (2) description and representation of objects as general second degree surfaces,
- (3) determination of the location and orientation of the objects with respect to a desired coordinate system,
- (4) performance of the rotation and translation transformations of the object so as to place it in a stable desired coordinate system,
- (5) use of the principle of two-dimensional discriminants to classify the various curves obtained by intersecting the surfaces with planes, and
- (6) acquisition of an optimal set of planes sufficient enough to distinguish and recognize each of the quadric surfaces. Angular bounds within which every surface yields a distinct set of curves are also determined in this step.

The range data, as mentioned in Section 1, is a pixel-by-pixel depth value from the point of origin of the laser to the point where the beam impinges on a surface. The objects are scanned from left-to-right and top-to-bottom. A grid frame may consist of 512 x 512 pixels. Before this range data is applied to the object classifier, it is median filtered and segmented.

As in our case [24], experiments were performed with square windows of mask sizes 3 x 3 and 5 x 5. Based upon certain curvature analysis, the 5 x 5 median filtered was found to be the most suitable for our purposes. Since isolated objects instead of complex scenes are considered, a simple thresholding whereby the object is separated from the background is utilized for the segmentation process. In the case where objects are irregular or a scene consists of a cluster of objects, Gaussian and mean curvatures have to be utilized to sub-divide the scene into planar or curved surfaces. Each surface is then recognized separately. Range image segmentation has been extensively studied by Levine et al. [11].

The processed range data is next utilized to obtain the quadric surface which best fits the data. Using the procedure described in [25], we determine the coefficients of a second degree polynomial representation for the three-dimensional surface. We assume that the data is a set of range-image samples obtained from a single surface which can be described by a quadric equation

$$F(x,y,z) = ax^2 + by^2 + cz^2 + 2fyz + 2gzx + 2hxy + 2px + 2qy + 2rz + d = 0, \quad (1)$$

where the values of the coefficients a , b , c , f , g , h , p , q , r , and d are known. Generally speaking, all of the objects in the experiments generate all ten coefficients as is shown in Section V. The question now is: How can we distinguish one object from the another and how accurately can we describe the recognized object? In the following sections of this section and Section IV, we describe the necessary scheme to solve the recognition problem of quadric surfaces.

4.2 Evaluation of the Rotation Matrix

The determination of the location and orientation of a three-dimensional object is one of the central problems in computer vision applications. It is observed that most of the methods and techniques which try to solve this problem require considerable pre-processing such as detecting edges or junctions, fitting curves or surfaces to segmented images and computing high order features from the input images. Since three-dimensional object recognition depends not only on the shape of the object but also the pose and orientation of the object as well, any definite information about the object's orientation will aid in selecting the right features for the recognition process.

In this section we suggest a method based on analytic geometry, whereby all the rotation parameters of any object placed in any orientation in space are determined and eliminated systematically. With this approach we are in a position to place the three-dimensional object in a desired stable position, thereby eliminating the orientation

problem. We can then utilize the shape information to explicitly represent the three-dimensional surface.

Any quadric surface can be represented by Equation (1) in terms of a second degree polynomial of variables x , y , and z .

The rotation parameters (product terms, $2f$, $2g$, and $2h$) after undergoing a set of sequential rotations about the three coordinate axes (rotational matrix formulated and described in Appendix 1), have the following representations:

$$2f'' = \left[(b \cdot \cos^2 \alpha + a \cdot \sin^2 \alpha + h \cdot \sin 2\alpha - c) \sin 2\beta + (2g \cdot \sin \alpha + 2f \cdot \cos \alpha) \cos 2\beta \right] \cos \gamma + \left[((b - a) \sin 2\alpha - 2h \cdot \cos 2\alpha) \cos \beta + (2g \cdot \cos \alpha - 2f \cdot \sin \alpha) \sin \beta \right] \sin \gamma. \quad (2)$$

$$2g'' = \sin 2\gamma \left[-\cos^2 \alpha (a - b \cdot \sin^2 \beta) - \sin^2 \alpha (-a \cdot \sin^2 \beta + b) + c \cdot \cos^2 \beta \right] + \sin 2\gamma \left[\sin 2\beta (f \cdot \cos \alpha + g \cdot \sin \alpha) + h \cdot \sin 2\alpha (1 + \sin^2 \beta) \right] + \cos 2\gamma \left[\sin 2\alpha \sin \beta (a - b) + 2h \cdot \sin \beta \cos 2\alpha + \cos \beta (2g \cdot \cos \alpha - 2f \cdot \sin \alpha) \right]. \quad (3)$$

$$2h'' = \sin 2\beta \sin \gamma [a \cdot \sin^2 \alpha + b \cdot \cos^2 \alpha - c + h \cdot \sin 2\alpha] + \cos 2\beta \sin \gamma [2g \cdot \sin \alpha + 2f \cdot \cos \alpha] + \cos \beta \cos \gamma [\sin 2\alpha (a - b) + 2h \cdot \cos 2\alpha] + \sin \beta \cos \gamma [2f \cdot \sin \alpha - 2g \cdot \cos \alpha]. \quad (4)$$

In order to eliminate the product terms $2f''$, $2g''$, and $2h''$, expressions (2) - (4) must be set equal to zero and solved simultaneously. As seen from these three expressions, each of them is a function of the rotation angles α , β , and γ . It is not possible to analytically find the rotation angles which eliminate the product terms. Instead, in the next section we present an iterative technique which performs the elimination of the product terms.

4.3 Product Terms Elimination Method

The product terms yz , xz , and xy in $F(x,y,z)$, denote the rotation terms which are to be eliminated. Elimination of all these rotation terms will place the three-dimensional surface on a coordinate system plane parallel to our coordinate system.

Observe that in the presence of a single rotation term, say yz , Equation (1) takes the form

$$F(x,y,z) = ax^2 + by^2 + cz^2 + 2fyz + 2px + 2qy + 2rz + d = 0.$$

The equation of the trace of the surface in the yz plane is obtained by setting $x = 0$. An appropriate rotation about the origin in the yz plane by an angle β will eliminate the yz term.

However, in the presence of two or more rotation terms, trying to eliminate a second rotation term will force the previously eliminated rotation term to reappear. Therefore, there will be at least two rotation terms present. The approach we propose is an iterative process, whereby at each stage the object is rotated in each of the coordinate planes, sequentially. The procedure is repeated until all the product terms are eliminated, i.e., the coefficients f , g , and h converge to zero in the limit.

Since our aim is to eliminate the rotation terms xy , yz , and xz , let's exclusively consider the coefficients of these rotation terms, namely f , g , and h evaluated in Section 3.2. In our iterative procedure we are able to eliminate all of the product terms. For example, suppose we wish to eliminate the term xy . By a specific rotation of α about the z axis, we will be able to accomplish our goal. However, while executing this process, the orientation of the object about the two planes yz and xz , i.e., the angles the object makes with these two planes have been changed. If we wish to eliminate the yz term, the object has to be rotated about the x axis by an angle β . Nevertheless, in this instance, while performing the process, the previously eliminated xy term reappears though the magnitude of its present orientation has been reduced. Hence by iterating the above process, an instance occurs when all the coefficients of the product terms converge to zero in the limit.

Consider the Equations (2), (3), and (4). First eliminate the coefficient h , i.e, the xy term. This can be accomplished by rotating the object about the z axis by an angle

α , whereas $\beta=\gamma=0$. Under these circumstances the new coefficients are as shown below.

$$2f_{11} = 2g \cdot \sin\alpha_1 + 2f \cdot \cos\alpha_1,$$

$$2g_{11} = 2g \cdot \cos\alpha_1 - 2f \cdot \sin\alpha_1,$$

and

$$2h_{11} = (a - b)\sin 2\alpha_1 + 2h \cdot \cos 2\alpha_1 = 0,$$

$$\text{where } \cot 2\alpha_1 = \frac{b - a}{2h}.$$

As seen above, the coefficient h has been forced to 0. The first digit of the subscript refers to the iteration number, whereas the second digit of the subscript denotes the number of times the object has been rotated by a specific angle. The remaining coefficients a , b , c , p , q , and r also reflect changes brought about by the above rotation.

The new coefficients are

$$a_{11} = a \cdot \cos^2\alpha_1 + b \cdot \sin^2\alpha_1 - 2h \cdot \sin\alpha_1 \cos\alpha_1,$$

$$b_{11} = b \cdot \cos^2\alpha_1 + a \cdot \sin^2\alpha_1 + 2h \cdot \sin\alpha_1 \cos\alpha_1,$$

$$c_{11} = c,$$

$$2p_{11} = 2p \cdot \cos\alpha_1 - 2q \cdot \sin\alpha_1,$$

$$2q_{11} = 2p \cdot \sin\alpha_1 + 2q \cdot \cos\alpha_1,$$

and

$$2r_{11} = 2r.$$

The new quadric equation is

$$F(x,y,z) = a_{11}x^2 + b_{11}y^2 + c_{11}z^2 + 2f_{11}yz + 2g_{11}xz + 2p_{11}x + 2q_{11}y + 2r_{11}z + d = 0.$$

Consider the second step wherein the coefficient corresponding to the yz term is forced to zero. In this particular case, the object has to be rotated by an angle β about the x axis, where $\alpha=\gamma=0$. Under these circumstances, the new rotation coefficients (signifying the product terms) become

$$2f_{12} = (b_{12} - c_{12})\sin 2\beta_1 + 2f_{11} \cdot \cos 2\beta_1 = 0,$$

$$\text{where } \cot 2\beta_1 = \frac{c_{11} - b_{11}}{2f_{11}},$$

$$2g_{12} = 2g_{11} \cdot \cos \beta_1,$$

and

$$2h_{12} = -2g_{11} \cdot \sin \beta_1.$$

At the same time the other coefficients become

$$a_{12} = a_{11},$$

$$b_{12} = c_{11} \cdot \sin^2 \beta_1 + b_{11} \cdot \cos^2 \beta_1 - 2f_{11} \cdot \sin \beta_1 \cos \beta_1,$$

$$c_{12} = b_{11} \cdot \sin^2 \beta_1 + c_{11} \cdot \cos^2 \beta_1 + 2f_{11} \cdot \sin \beta_1 \cos \beta_1,$$

$$2p_{12} = 2p_{11},$$

$$2q_{12} = 2q_{11} \cdot \cos \beta_1 - 2r_{11} \cdot \sin \beta_1,$$

and

$$2r_{12} = 2q_{11} \cdot \sin \beta_1 + 2r_{11} \cdot \cos \beta_1.$$

The new quadric equation is:

$$F(x,y,z) = a_{12}x^2 + b_{12}y^2 + c_{12}z^2 + 2g_{12}xz + 2h_{12}xy + 2p_{12}x + 2q_{12}y + 2r_{12}z + d = 0.$$

In the final step of the initial iteration, the coefficient corresponding to the xz term is forced to zero. In this case, the object is to be rotated by an angle γ about the y axis, whereas $\alpha=\beta=0$. Under these circumstances, the new rotation coefficients becomes

$$2f_{13} = 2h_{12} \cdot \sin\gamma_1 = -2g_{11} \cdot \sin\beta_1 \sin\gamma_1,$$

$$2g_{13} = (a_{13} - c_{13})\sin 2\gamma_1 + (2g_{11} \cdot \cos\alpha_1 - f_{11} \cdot \sin\alpha_1)\cos\beta_1 \cos 2\gamma_1 = 0,$$

$$\text{where } \cot 2\gamma_1 = \frac{c_{13} - a_{13}}{2g_{12}},$$

and

$$2h_{13} = 2h_{12} \cdot \cos\gamma_1 = -2g_{11} \cdot \sin\beta_1 \cos\gamma_1.$$

Let's now carefully analyze the coefficients of xy , yz , and zx obtained in the final step of the first iteration. Consider, for instance, the coefficient corresponding to the yz term. It is observed that while proceeding from one step to the other, the new coefficients are getting multiplied by the sine or cosine of the concerned angle. This implies that in every succeeding step these coefficients are decreasing in their magnitude. To justify the above statement, let us now consider all the coefficients obtained in the second iteration.

At the end of stage 1 of the second iteration, the rotation coefficients become

$$2f_{21} = 2f_{13} \cdot \cos\alpha_2 = -2g_{11} \cdot \sin\beta_1 \sin\gamma_1 \cos\alpha_2,$$

$$2g_{21} = -2f_{13} \cdot \sin\alpha_2 = 2g_{11} \cdot \sin\beta_1 \sin\gamma_1 \sin\alpha_2,$$

and

$$2h_{21} = 0, \text{ where } \cot 2\alpha_2 = \frac{b_{13} - a_{13}}{2h_{13}}.$$

At the end of the second stage of the second iteration, the rotation coefficients become

$$2f_{22} = 0 \text{ where } \cot 2\beta_2 = \frac{c_{21} - b_{21}}{2f_{21}},$$

$$2g_{22} = 2g_{11} \cdot \sin\beta_1 \sin\gamma_1 \sin\alpha_2 \cos\beta_2,$$

and

$$2h_{22} = -2g_{11} \cdot \sin\beta_1 \sin\gamma_1 \sin\alpha_2 \sin\beta_2.$$

Similarly at the end of the final stage of the second iteration, the rotation coefficients reduce to

$$2f_{23} = -2g_{11} \cdot \sin\beta_1 \sin\gamma_1 \sin\alpha_2 \sin\beta_2 \sin\gamma_2,$$

$$2g_{23} = 0 \text{ where } \cot 2\alpha_2 = \frac{b_{13} - a_{13}}{2h_{13}},$$

and

$$2h_{23} = -2g_{11} \cdot \sin\beta_1 \sin\gamma_1 \sin\alpha_2 \sin\beta_2 \cos\gamma_2.$$

The terms α_2 , β_2 , and γ_2 are the respective rotation angles along the z, x, and y axes in the second iteration. Hence it is observed with each iteration that the rotation coefficients get smaller and smaller in magnitude and eventually disappear in the limit.

Once the rotation terms, i.e., xy , yz , and xz are eliminated, the three-dimensional surface has the representation of

$$F(x,y,z) = Ax^2 + By^2 + Cz^2 + 2Px + 2Qy + 2Rz + D = 0, \quad (5)$$

where A, B, C, P, Q, and R are the coefficients resulting after the elimination of the rotation terms. A natural question to ask is: Can the terms of the first degree be eliminated by means of a translation? The answer is sometimes they can and sometimes

they cannot. The case, where the term can be eliminated, is supported by the following theorem.

Theorem 1. The terms of the first degree of an equation of a quadric surface can be eliminated by means of a translation if and only if the surface has a center, in which case the first degree terms are eliminated if and only if the new origin is a center [26].

All of the above procedures performed until now result in a second degree polynomial describing an unknown object, the center of the object lying at the origin of our coordinate system. Had the test data been simulated, the three-dimensional discriminant approach which was mentioned in Section 1 could be used to describe and recognize the object. Since the test data is not simulated, we should utilize a recognition algorithm which will distinguish and recognize each of the test surfaces from one another.

The intersection of a surface with a plane generates a curve. The nature of this curve depends solely on what type of object is intersected and with which particular plane and in which orientation. Since we have no knowledge of the surface type, a priori, one approach is to intersect the surface with a series of planes. We need to determine the optimum number of planes which will uniquely characterize each of the quadric surfaces.

Our goal is to derive a consistent method for determining the minimum number of planes necessary to intersect a given quadric surface so that the generated conics uniquely characterize the surface. This goal includes the derivation and formulation of the angular bounds for which a particular plane intersecting a surface generates the same two-dimensional curve. In summary, each of the quadric surfaces is represented by a unique five-tuple, whose elements signify the presence or absence of the following curves: circle, ellipse, hyperbola, parabola, and a line.

5. QUADRIC SURFACE CHARACTERIZATION AND RECOGNITION

Our proposed method utilizes a two-dimensional discriminant which is a measure for distinguishing curves. Since the ten generated coefficients described in Section 3 give a three-dimensional representation of the surfaces, we propose to identify the quadrics using the information resulting from the intersection of the surface with different planes. If the surface is one of those considered for the recognition process (see figures 2, 3, and 4), there are five possible two-dimensional curves that may result from such intersections: (i) a circle, (ii) an ellipse, (iii) a parabola, (iv) a hyperbola, and (v) a line. Thus, a feature or pattern vector with five independent components can be formed for characterizing each of the surfaces.

The three-dimensional surfaces (objects) to be recognized are listed below:

- (a) an ellipsoid,
- (b) a circular cylinder,
- (c) a sphere,
- (d) a quadric cone,
- (e) a hyperboloid of one sheet,
- (f) a hyperboloid of two sheets,
- (g) an elliptic paraboloid,
- (h) a hyperbolic cylinder,
- (i) a parabolic cylinder,
- (j) a hyperbolic paraboloid, and
- (k) a parallelepiped.

As discussed in Section 3.2, we now assume that the three-dimensional objects have undergone two basic transformations, rotation and translation. Consequently the product terms in the representation $F(x,y,z)$ for a particular surface have been eliminated and the center of the surface lies at the origin of our specified coordinate sys-

tem. As illustrated in figures 2, 3, and 4, all of the surfaces are contained in the xy plane with their centers at O (the origin). For each surface, the characterization is performed in two steps. Initially we consider the intersection of each object with two planes (horizontal and vertical). This step does not require that the surface undergoes a translation transformation. We refer to plane 1 as the one that intersects the object parallel to the xy plane, i.e., z constant. Also refer to plane 2 as the one that intersects the object parallel to the xz plane, i.e., y constant. In the second step, the minimum set of intersecting planes needed to yield a unique feature vector (the various curves serve as features) is determined. In this step we assume that the object has undergone the translation transformation. Next we consider the representation procedure for the quadric cone which is similarly conducted for each of the remaining surfaces.

Step 1:

The general representation of a circular cone on a plane parallel to the xy plane and its axis of revolution parallel to the z axis is

$$F(x,y,z) = bx^2 + by^2 + cz^2 + 2px + 2qy + 2rz + d = 0, \quad (6)$$

where $bc < 0$ and $d = \frac{p^2}{b} + \frac{q^2}{b} + \frac{r^2}{c}$.

From Equation (6), upon completing squares, we have

$$F(x,y,z) = b\left[x + \frac{p}{b}\right]^2 + b\left[y + \frac{q}{b}\right]^2 + c\left[z + \frac{r}{c}\right]^2 + d - \frac{p^2}{b} - \frac{q^2}{b} - \frac{r^2}{c} = 0. \quad (7)$$

Since $d = \frac{p^2}{b} + \frac{q^2}{b} + \frac{r^2}{c}$, Equation (7) becomes

$$F(x,y,z) = \frac{\left[x + \frac{p}{b}\right]^2}{\frac{1}{b}} + \frac{\left[y + \frac{q}{b}\right]^2}{\frac{1}{b}} - \frac{\left[z + \frac{r}{c}\right]^2}{\frac{-1}{c}} = 0. \quad (8)$$

In the case of the elliptic cone, Equation (8) reduces to

$$F(x,y,z) = \frac{\left[x + \frac{p}{a}\right]^2}{\frac{1}{a}} + \frac{\left[y + \frac{q}{b}\right]^2}{\frac{1}{b}} - \frac{\left[z + \frac{r}{c}\right]^2}{\frac{-1}{c}} = 0, \quad (9)$$

where $ab > 0$, $ac < 0$, and $bc < 0$. If $c < 0$, i.e., $b > 0$, the intersection of the cone represented by Equation (8) with plane 1, i.e., $z = k$, where $\frac{-r}{c} - \sqrt{\frac{-1}{c}} < k < \frac{-r}{c} + \sqrt{\frac{-1}{c}}$, would generate

$$\frac{\left[x + \frac{p}{b}\right]^2}{\frac{1}{b}} + \frac{\left[y + \frac{q}{b}\right]^2}{\frac{1}{b}} = \frac{\left[k + \frac{r}{c}\right]^2}{\frac{-1}{c}}, \quad (10)$$

where $\frac{1}{c}$ is a positive quantity. The above equation is that of a circle. The elliptic cone on the other hand which is represented by Equation (9), upon intersection with plane 1, i.e., $z = k$, where $\frac{-r}{c} - \sqrt{\frac{-1}{c}} < k < \frac{-r}{c} + \sqrt{\frac{-1}{c}}$, would generate

$$\frac{\left[x + \frac{p}{a}\right]^2}{\frac{1}{a}} + \frac{\left[y + \frac{q}{b}\right]^2}{\frac{1}{b}} = \frac{\left[k + \frac{r}{c}\right]^2}{\frac{-1}{c}}, \quad (11)$$

which is an ellipse. The intersection of the circular cone with plane 2, i.e., $y=k$, where $\frac{-q}{b} - \sqrt{\frac{1}{b}} < k < \frac{-q}{b} + \sqrt{\frac{1}{b}}$, would generate

$$\frac{\left[x + \frac{p}{b}\right]^2}{\frac{1}{b}} - \frac{\left[z + \frac{r}{c}\right]^2}{\frac{-1}{c}} = \frac{\left[k + \frac{q}{b}\right]^2}{\frac{1}{b}}, \quad (12)$$

where $-\frac{1}{c}$ is a positive quantity. Equation (12) represents a hyperbola. A similar result is obtained when the elliptic cylinder is intersected with plane 2.

Step 2:

The quadric representation of the elliptic cone illustrated in Figure 5 is

$$\frac{X^2}{A^2} + \frac{Y^2}{B^2} - \frac{Z^2}{C^2} = 0. \quad (13)$$

Intersection of the cone with horizontal planes $z = k$, where $-c < k < c$, generates ellipses as intercepts. Let us consider the horizontal plane $Z = -C$ and determine the various intercepts formed by its inclined sub-planes. The equation of the plane passing through the points $E(A,0,-C)$, $F(0,-B,-C)$, and $G(0,0,L)$ where $-C < L < C$, is

$$-A(C+L)Y + ABZ + B(C+L)X - ABL = 0.$$

Substituting Z in Equation (13) results in

$$B^2[C^2 - (C+L)^2]X^2 + A^2[C^2 - (C+L)^2]Y^2 - 2AB(C+L)^2XY + \dots = 0,$$

thereafter,

$$\delta = 4A^2B^2[(C+L)^4 - (L^2+2LC)^2].$$

Analyzing δ leads to the following bounds:

For $L \geq 0$ the intersections are hyperbolas.

For all values of L , $-C < L < 0$, except for $L = -C + \frac{C}{\sqrt{2}}$, the intersections are ellipses.

For the one particular case where $L = -C + \frac{C}{\sqrt{2}}$, the intersection is a parabola. In terms of θ , the angle between the $Z = -C$ plane and its inclined sub-plane is

$$\cos\theta = \frac{AB}{\sqrt{A^2(C+L)^2 + A^2B^2 + B^2(C+L)^2}}.$$

DETAILED VIEW : HORIZONTAL INTERSECTIONS

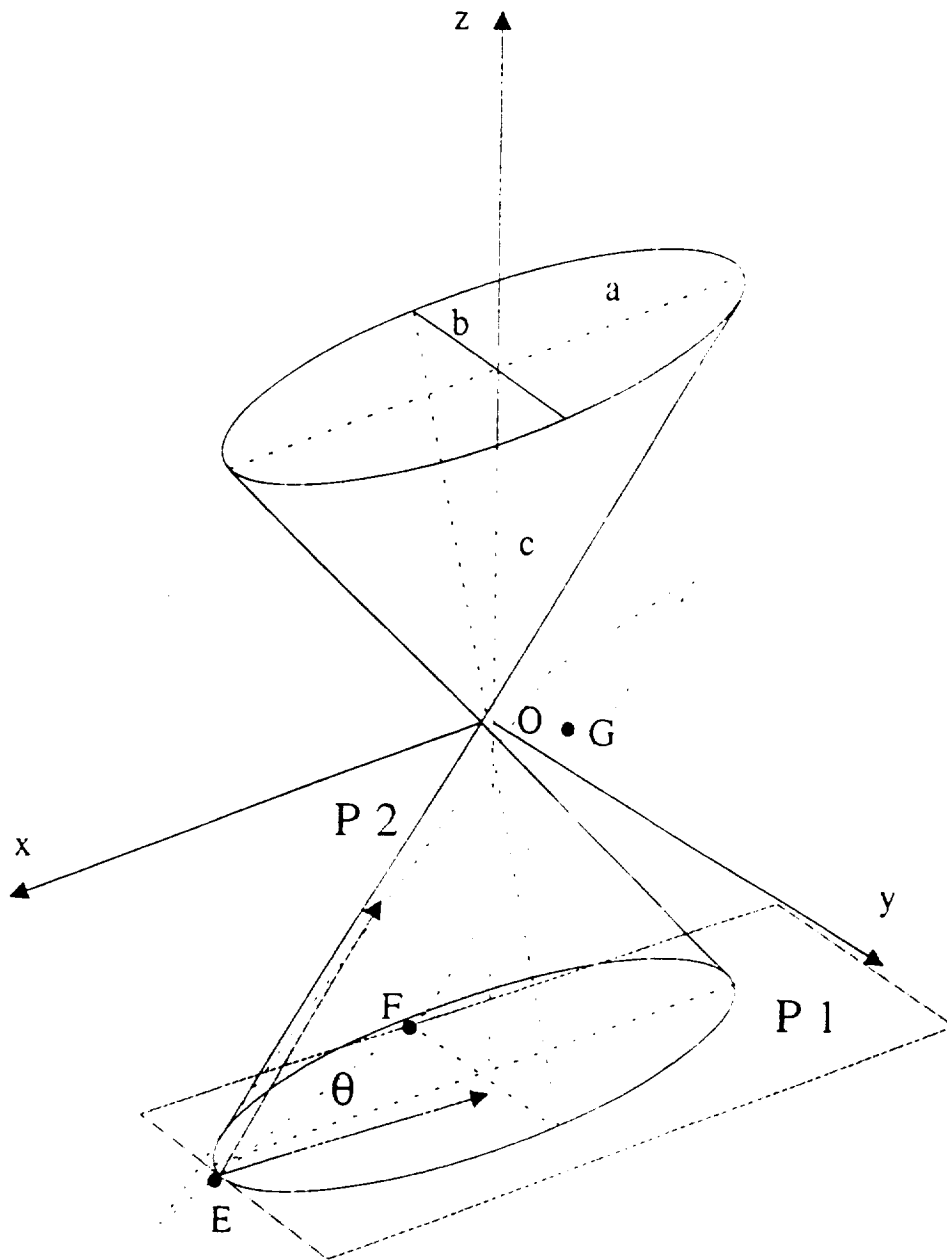


Figure 5. Plane P1 and planes parallel to it within the range $-c$ to c (except the one passing through the origin) generate ellipses. Plane P2 is the inclined sub-plane which denotes the maximum inclination or range (of plane P1) within which ellipses are generated. θ is the angular bound in terms of the angle.

Next, consider the intersections formed by the plane $X = 0$ and its sub-planes. Substituting $X = 0$ in Equation (13) leads to the intersection

$$\frac{Y^2}{B^2} - \frac{Z^2}{C^2} = 0,$$

which is a degenerate hyperbola. For all $-A < X < A$, the intercepts are hyperbolas.

The equation of the plane passing through the points $H(0,-B,-C)$, $I(0,B,-C)$, and $J(L,0,C)$, where $L > 0$ is

$$LZ - 2CX + LC = 0.$$

Solving for Z and substituting in Equation (13) leads to the representation of the intercept as

$$X^2[L^2 - 4A^2]B^2 + L^2A^2Y^2 + 4A^2B^2XL + \dots = 0. \quad (14)$$

Solving $L^2 - 4A^2$, indicates the following conditions for the various intercepts:

For $L = 2A$, the intercept is a parabola.

For all values of L , $-2A < L < 2A$, the intercepts are hyperbolas.

For all $L > 2A$, the intercepts are ellipses.

Figure 6 illustrates all of the above results. The angle between the $X = 0$ plane and its inclined sub-planes for the above obtained interceptions is

$$\cos\theta < \frac{+2C}{\sqrt{(L^2 + 4C^2)}}.$$

Figure 7 shows a lateral view of all possible curves intercepted in a quadric cone by the various planes. Table 1 summarizes the results obtained for the quadric cone. Table 2 lists out the various discriminants obtained which aid in differentiating the several quadric surfaces. The variables A , B , C , L , and K signify the radius and height of the quadric surfaces.

DETAILED VIEW : VERTICAL INTERSECTIONS

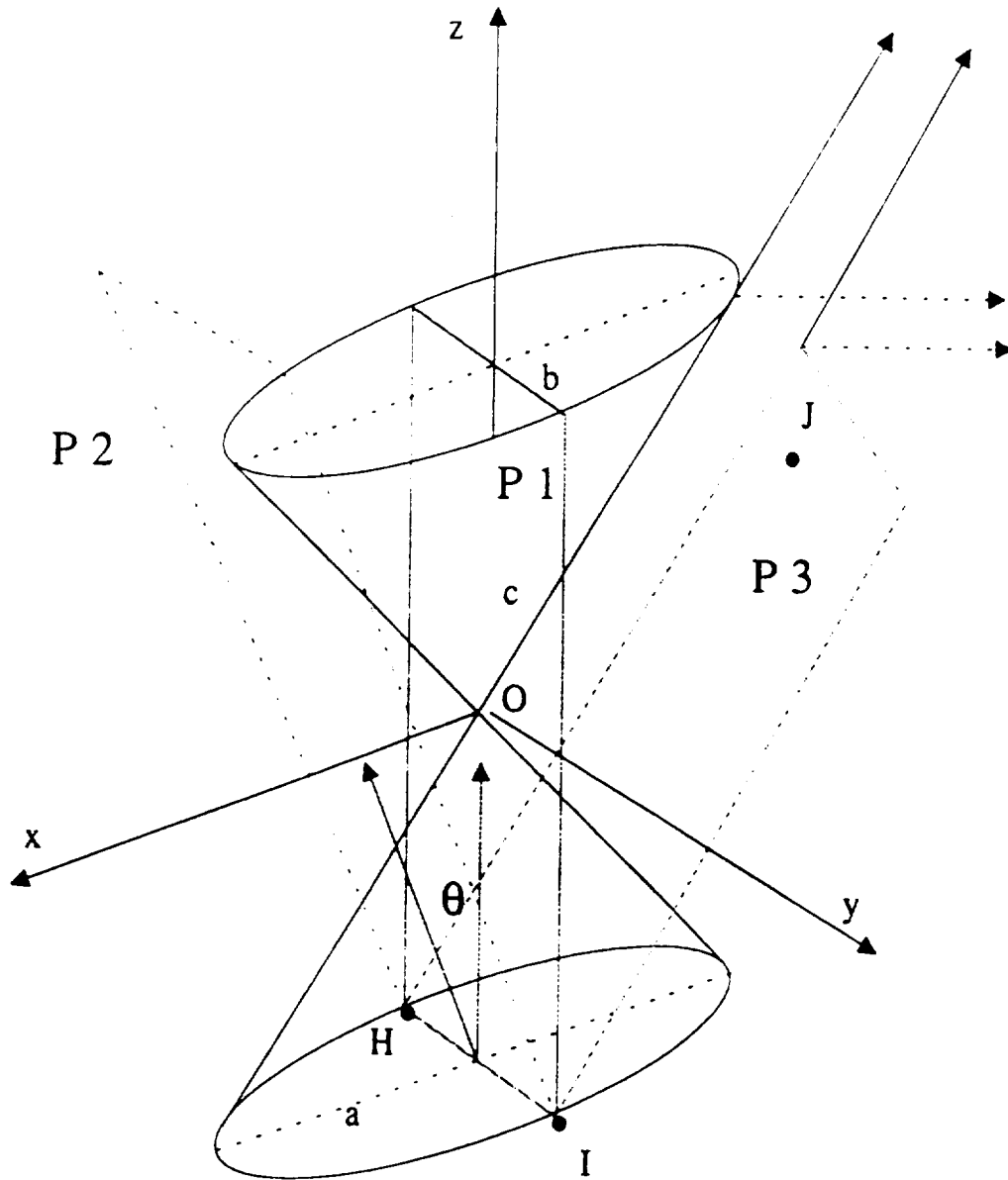


Figure 6. Plane P1 and planes parallel to it within the range $-b$ to b generates degenerate hyperbolas. Plane P2 is the inclined sub-plane which shows the outer region or the maximum inclination (of plane P1) within which hyperbolas are intercepted. θ is the angular bound in terms of the angle. Plane P3 is the only exception where the intersection is a parabola. In this case the inclination of the plane P3 is equal to the base angle of the cone.

LATERAL VIEW

INTERSECTION OF A PLANE AND A CONE

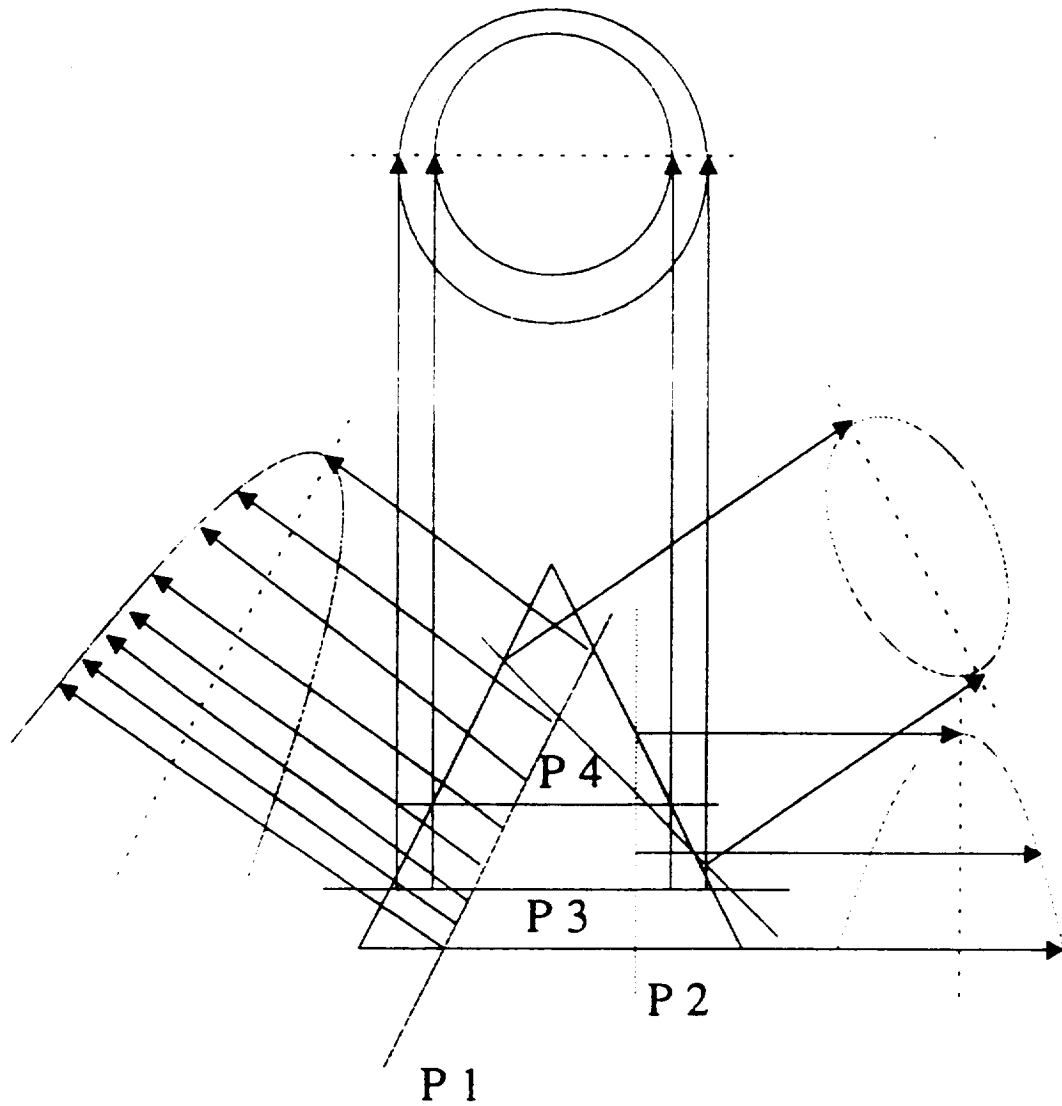


Figure 7. P1, P2, P3, and P4 are the four planes which generate all the intersections with the quadric cone. Plane P1 which has the same base angle as that of the cone intercepts a parabola. Plane P2 intercepts a hyperbola. Plane P3 intercepts a circle and finally plane P4 intercepts an ellipse. (The quadric cone under question has a circular base).

PLANE	INTERSECTION
$Z = K$	Circle, Ellipse
$X = K$	Hyperbola
Inclined sub-planes of $Z=K, L \geq 0$	Hyperbolas
Inclined sub-planes of $Z=K, -C < L < 0$	Ellipses
Inclined sub-planes of $Z=K, L = -C + \frac{C}{\sqrt{2}}$	Parabola
Inclined sub-planes of $X=K, L = 2A$	Parabola
Inclined sub-planes of $X=K, L < 2A$	Hyperbolas
Inclined sub-planes of $X=K, L > 2A$	Ellipses

Table 1. Intersection of quadric cone with planes.

Table 3 summarizes the various curves (conics) derived from intersecting each of the eleven surfaces with the two planes $z = k$ and $y = k$. These observations follow the results obtained in step 1 of each of the quadric surfaces. As seen from Table 3, the quadric cone and the hyperboloid of one and two sheets all generate similar curves. However, after using the results of step 2 (where angular bounds have been determined), we are able to distinguish each of the quadric surfaces from one another. Each of the quadric surfaces can be represented by a binary five-tuple, where the numeral 1 indicates the presence of a particular curve and the numeral 0 refers to the non-existence of that curve. Table 4 presents the feature vector for each of the quadric surfaces.

Quadric surfaces which seem to have identical feature vectors in the table above, get differentiated when the angular bounds theory as defined and derived for each of the surfaces (step 2) is applied.

DISCRIMINANTS	ANGULAR BOUND	CURVE	SURFACE
$\delta = 4A^2B^2 - C^4 - 2C^2K^2$		ellipse	ellipsoid
$\delta = 4B^2K^2$	$\cos\theta \leq \frac{2AB}{\sqrt{A^2K^2 - 4A^2B^2 - B^2K^2}}$	ellipse	elliptic cylinder
$\delta = \frac{-K^2}{L^2A^2B^2}$	$\cos\theta < \frac{2L}{\sqrt{A^2 - 4K^2}}$	ellipse	elliptic cylinder
$\delta = -4A^2(1-2K^2)$		circle	sphere
$\delta = 4A^2B^2(C-L)^4 - (L^2-2LC)^2$	$\cos\theta = \frac{AB}{\sqrt{(A^2(C-L)^2 - A^2B^2 - B^2(C-L)^2)}}$	hyperbola, ellipse, parabola	quadric cone
$\delta = -4A^2L^2(L^2-4A^2)$	$\cos\theta < \frac{2C}{\sqrt{(L^2 - 4C^2)}}$	parabola, hyperbola, ellipse	quadric cone
$\delta = 4A^2B^2A^2 - K^2 - 2AK(A^2 - K^2 - 2AK)$	$\cos\theta = \frac{B(A-K)}{\sqrt{B^2(A-K)^2 - A^2C^2 - B^2C^2}}$	parabola, hyperbola, ellipse	hyperboloid of one sheet
$\delta = 4A^2B^2(L^2A^2C - K)^4 - (C^2(L-M)^2 - A^2(C-K)^2)(C^2(L-M)^2 - L^2C - K)^2$	$\cos\theta = \frac{B(L-M)}{\sqrt{B^2(C-K)^2 - L^2(C-K)^2 - B^2(L-M)^2}}$	parabola, hyperbola, ellipse	hyperboloid of one sheet
$\delta = -4A^2K^2(K^2-4A^2)$	$\cos\theta < \frac{2C}{\sqrt{K^2 - 4C^2}}$	hyperbola, parabola, ellipse	hyperboloid of one sheet
$\delta = 4A^2B^2(T-L)^4 - (C^2 - (T-L)^2)^2$	$\cos\theta = \frac{AB}{\sqrt{(A^2(T-C)^2 - A^2B^2 - B^2(T-C)^2)}}$	parabola, hyperbola, ellipse	hyperboloid of two sheets
$\delta = -4A^2L^2C^2B^2L^2C^2 - 4A^2T^2$	$\cos\theta = \frac{2T}{\sqrt{L^2 - 4T^2}}$	parabola, hyperbola, ellipse	hyperboloid of two sheets
$\delta = \frac{-4}{A^2B^2}$	$\cos\theta \leq \frac{AB}{\sqrt{(A^2K-L)^2 - A^2B^2 - B^2(L-K)^2}}$	ellipse	elliptic paraboloid
$\delta = \frac{-4A^2}{A^2B^2(L-M)^2}$	$\cos\theta < \frac{(L-M)}{\sqrt{(N^2 - (L-M)^2)}}$	ellipse	elliptic paraboloid

Table 2. Discriminants and bounds associated with the various quadric surfaces.

OBJECT	PLANE 1 : $x = k$	PLANE 2 : $y = k$
Ellipsoid	Ellipse	Circle
Circular cylinder	Circle	Line
Sphere	Circle	Circle
Quadric cone	Circle	Hyperbola, Parabola
Hyperboloid of one sheet	Circle	Hyperbola, Parabola
Hyperboloid of two sheets	Circle, Point	Hyperbola, Parabola
Elliptic paraboloid	Ellipse	Parabola
Hyperbolic cylinder	Hyperbola	Line
Parabolic cylinder	Line	Parabola
Hyperbolic paraboloid	Hyperbola	Line
Parallelepiped	Line	Line

Table 3. The various curves intercepted by the quadric surfaces when intersected with the planes $z = k$ and $y = k$.

3-D SURFACE	CIRCLE	ELLIPSE	PARABOLA	HYPERBOLA	LINE
Ellipsoid	1	1	0	0	0
Circular cylinder	1	1	0	0	1
Sphere	1	0	0	0	0
Quadric cone	1	1	1	1	1
Hyperboloid of one sheet	1	1	1	1	0
Hyperboloid of two sheets	1	1	1	1	0
Elliptic paraboloid	1	1	1	0	0
Hyperbolic cylinder	0	0	0	1	1
Parabolic cylinder	0	0	1	0	1
Hyperbolic paraboloid	0	0	1	1	1
Parallelepiped	0	0	0	0	1

Table 4. Feature vectors (representing the presence or absence of curves) for each of the quadric surfaces.

6. EXPERIMENTAL RESULTS

Range images were obtained using the Laser-Range-Mapper. The range image sensor is based upon FMCW coherent laser radar (CLR) systems previously developed by the Digital Signal Division of Coleman Research Corporation [27]. In these systems, a laser diode source is frequency chirped via its injection current such that the output optical frequency is swept linearly as a function of time. The laser output is divided and used both as a local oscillator (LO) and as the signal to be transmitted. After being time delayed by the round trip transit time to the target, the received signal is mixed with the optical LO on a photodiode. The resultant beat frequency is equal to the optical signal multiplied by the time delay between the received signal and the local oscillator. Since this time delay is proportional to the target distance, the RF beat frequency is also proportional to the target distance. Most of the processing and computations were conducted on a Micro Vax 750 system.

The experimental work was performed in the following order :

- (i) The effect of median filtering on range images was studied.
- (ii) The proposed recognition scheme was applied to filtered range images.
- (iii) The quadric alignment algorithm was applied to simulated and real data.
- (iv) The three-dimensional discriminant approach was tested with simulated data.

Range images of objects like spheres, cylinders and cones were segmented in order to separate the object from its background. The resulting image, which is referred to as the raw image, was then median filtered with mask size 5×5 . Once the data files were obtained for each of the filtered images, the depth information of each of these files was converted into rectangular coordinates. The operation manual for the laser radar three-dimensional vision system [27] describes the equations used for the transformations of the range information from spherical coordinates to rectangular coordinates:

$$X = (R - L)\sin\theta_f,$$

$$Y = (R - \frac{\delta}{\cos\theta_f} - L)\sin\theta_g\cos\theta_f,$$

and

$$Z = (R - \frac{\delta}{\cos\theta_f} - L)\cos\theta_g\cos\theta_f,$$

where θ_f is the horizontal scanning angle and θ_g is the vertical scanning angle.

$$\theta_f = 25^\circ - (\text{horizontal pixel \#}) (0.1961 \text{ deg/pixel}).$$

$$\theta_g = (\text{vertical pixel \#}) (0.1961 \text{ deg/pixel}) - 25^\circ.$$

$$L = 0.362\text{m}.$$

$$R \text{ is Range in meters} = (0.00459 \text{ m/pixel})(\text{Range pixel}) + (n - 1/2),$$

where n is the electronic range in meters set by the operator. The cartesian coordinate information was then utilized for determining the coefficients which describe each of the three-dimensional surfaces.

Experiments were conducted on real range data for spheres and cylinders and cones. Consider the case of the cylinder shown in Figure 8. The coefficients of the general equation for a 5 x 5 filtered image were

$$a = 0.0572$$

$$b = 0.599$$

$$c = 0.4416$$

$$2f = -0.807$$

$$2g = 0.459$$

$$2h = -0.149$$

$$2p = -0.5915$$

$$2q = 1.089$$



Figure 8. Processed range image of a pipe which is described and recognized as a cylindrical surface.

$$2r = -1.019$$

$$d = 0.664$$

These coefficients by themselves do not come any close in describing the cylinder. However, after utilizing the alignment algorithm, a entirely new set of coefficients as shown below is generated.

$$a = -0.07251$$

$$b = 0.977$$

$$c = 0.1930$$

$$2f = 0.0$$

$$2g = 0.0$$

$$2h = 0.0$$

$$2p = -0.1764$$

$$2q = 1.5696$$

$$2r = -1.1902$$

$$d = 0.664$$

Three iterations were needed to eliminate the product terms. The rotation matrix was found to be

$$\begin{bmatrix} 0.806 & 0.3 & -0.5 \\ 0.1032 & 0.764 & 0.636 \\ 0.581 & -0.565 & 0.584 \end{bmatrix},$$

from which the orientation of the cylinder with respect to our coordinate system was determined to be

$$\begin{bmatrix} -12.18^\circ \\ 34.33^\circ \\ 41.91^\circ \end{bmatrix}.$$

When these angles of α , β , and γ were plugged back in the expressions of the product terms, f , g , and h , respectively, all converged to zero in the limit. This result validated

our alignment technique. Step 1 of the feature extraction mode results in line being intercepted when the surface is intersected with the plane $y = k$. Plane $z = k$ on the other hand intercepts an ellipse. Utilizing the set of planes derived earlier, the object is classified as a cylinder. Proceeding further, using the coefficients of the 5×5 filtered image of the cylinder, the diameter of this particular cylinder was calculated to be 4.99 centimeters. The actual diameter of the cylinder was 5.08 centimeters.

A similar set of coefficients obtained from the 5×5 filtered image of a quadric cone are as listed next:

$$a = 0.995$$

$$b = -0.034$$

$$c = -0.008493$$

$$2f = 0.0504$$

$$2g = -0.1104$$

$$2h = -0.04773$$

$$2p = 0.009587$$

$$2q = -0.001688$$

$$2r = 0.006907$$

$$d = -.010696$$

After the rotation alignment technique is applied, the above set of coefficients change to

$$a = 0.688$$

$$b = 0.3408$$

$$c = -1.09$$

$$2f = 0.0$$

$$2g = 0.0$$

$$2h = 0.0$$

$$2p = -0.124$$

$$2q = 0.296$$

$$2r = -0.0902$$

$$d = 0.0789$$

Three iterations were needed to eliminate the product terms. The rotation matrix was found to be

$$\begin{bmatrix} 0.99 & 0.0476 & -0.04168 \\ -0.0199 & 0.86 & 0.506 \\ 0.06 & -0.505 & 0.861 \end{bmatrix},$$

from which the orientation of the cylinder with respect to our coordinate system was determined to be

$$\begin{bmatrix} -0.21^\circ \\ 28.985^\circ \\ 2.77^\circ \end{bmatrix}.$$

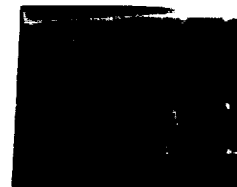
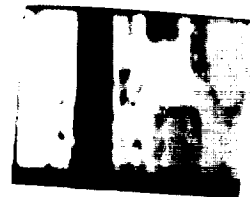
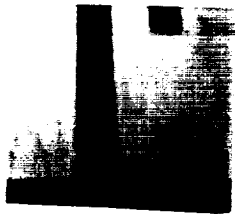
When these angles of α , β , and γ were inserted back in the expressions of the product terms, f , g , and h , respectively, all converged to zero in the limit. This result validated our alignment technique. Step 1 of the feature extraction mode results in a ellipse being intercepted when the surface is intersected with the plane $y = k$. Plane $z = k$ on the other hand intercepts an hyperbola. Utilizing the set of planes derived earlier, the object is classified as a quadric cone with an elliptic base. Proceeding further, using the coefficients of the 5×5 filtered image of the cone, the diameter of this particular cylinder was calculated to be 10.12 centimeters. The actual diameter of the cylinder was 9.98 centimeters.

Experiments were carried out for four sets of other real range images of spheres, cylinders, and quadric cones. In all of these cases the surfaces were correctly recognized after utilizing the discriminants and the angular bound information listed in Table 2.

The rotation alignment technique was utilized for a large group of simulated data. Listed in Tables 5, 6, 7 and are several upon which the utilization of our recognition scheme correctly identified the surfaces. Upon application of our recognition scheme the quadric surfaces represented in Tables 5, 6, and 7 were correctly recognized as an ellipsoid, a hyperboloid of one sheet, and a hyperbolic cylinder, respectively.

All the simulated data sets of quadric surfaces could be recognized after conducting the rotation alignment technique on the original quadratic representation.

Experimental results for the newly proposed segmentation scheme is discussed next. Shown in Figure 9(a) is a range image of a printed circuit board (PCB). Utilizing a edge detector schme based upon gradient information, two types of edges are determined. Figure 9(b) is the edge-image along the y-direction, whereas Figure 9(c) is the edge-image along the x-direction. A step edge-image is formed by overlaying images in figures 9(a) and (b). Next a thinning algorithm is utilized to thin edges to a pixel thick. Unwanted edges and streaks of salt and pepper noise is eliminated using a median filter of size 5 x 5. Figure 9(d) illustrates this new image. Next utilizing the blob finding technique various enclosed areas, each reflecting a surface is determined, and subsequently mapped. The resultant image is shown in Figure 9(e). The mapped images can now be utilized for the recognition scheme which was described in vast detail in sections 4 and 5.



COEFFICIENT	BEFORE	AFTER ALIGNMENT
A, COEFF. OF X^2	103	49.84
B, COEFF. OF Y^2	125	96.887
C, COEFF. OF Z^2	66	145.3905
F, COEFF. OF YZ	-60	0.0
G, COEFF. OF XZ	-12	0.0
H, COEFF. OF XY	-48	0.0
P, COEFF. OF X	0.0	0.0
Q, COEFF. OF Y	0.0	0.0
R, COEFF. OF Z	0.0	0.0
D, CONSTANT	-294	-294

Table 5. New coefficients of an unknown simulated data obtained after alignment.

COEFFICIENT	BEFORE	AFTER ALIGNMENT
A, COEFF. OF X^2	0.0	2.0
B, COEFF. OF Y^2	2.0	-4.0
C, COEFF. OF Z^2	1.0	-1.0
F, COEFF. OF YZ	-4.0	0.0
G, COEFF. OF XZ	-4.0	0.0
H, COEFF. OF XY	0.0	0.0
P, COEFF. OF X	0.0	0.0
Q, COEFF. OF Y	0.0	0.0
R, COEFF. OF Z	0.0	0.0
D, CONSTANT	-4.0	-4.0

Table 6. New coefficients of an unknown simulated data obtained after alignment.

COEFFICIENT	BEFORE	AFTER ALIGNMENT
A, COEFF. OF X^2	0.0	3.0
B, COEFF. OF Y^2	0.0	0.0
C, COEFF. OF Z^2	0.0	-3.0
F, COEFF. OF YZ	-1.414	0.0
G, COEFF. OF XZ	0.0	0.0
H, COEFF. OF XY	1.0	0.0
P, COEFF. OF X	0.0	0.0
Q, COEFF. OF Y	0.0	0.0
R, COEFF. OF Z	0.0	0.0
D, CONSTANT	-3.0	-3.0

Table 7. New coefficients of an unknown simulated data obtained after alignment.

6. CONCLUSIONS

We have presented a new approach based on two-dimensional analytic geometry to recognize a series of three-dimensional objects. Among the various three-dimensional objects considered are the hyperboloids of one and two sheets, the ellipsoids, the spheres, the circular and elliptical quadric cones, the circular and elliptical cylinders, the parabolic and hyperbolic cylinders, the elliptic and hyperbolic paraboloids, and the parallelepipeds. Our proposed method utilizes a two-dimensional discriminant which is a measure for distinguishing curves. Instead of evaluating the ten generated coefficients and attempting to recognize the surface from its quadric representation, we can identify the quadrics using the information resulting from the intersection of the surface with different planes. If the surface is one of those listed above, there are five possible two-dimensional curves that may result from such intersections: (i) a circle, (ii) an ellipse, (iii) a parabola, (iv) a hyperbola, and (v) a line. Thus, a feature or pattern vector with five independent components can be formed for characterizing each of the surfaces. Although all of the quadric surfaces considered have been symmetric, our recognition system can be extended to other three-dimensional objects. To recognize complex objects a suitable segmentation technique has been developed and implemented for the isolation of each individual surface.

Some of the advantages of our recognition scheme are listed below:

- (1) Recognition systems using the curvature approach (evaluation of the mean and Gaussian curvatures) are very computationally intensive. These approaches never really describe the quadric surface in question. Our proposed recognition system is computationally efficient. All of the quadric surfaces are recognized as well as described in terms of their dimensions.
- (2) Unlike some of the traditional techniques which perform well only on simulated,

Our recognition system is shown to work for both simulated and real range data.

(3) The best-fit plot and the curvature analysis techniques [24] used for analyzing processed range images can be used to determine performances of various laser range mappers.

(4) The rotation alignment technique is a new method which systematically and effectively eliminates the product terms and aligns the quadric surfaces in our desired coordinate system through an iterative technique.

(5) Although intersections of surfaces with planes has been looked into before, only in this research a complete set of features for the recognition of all the quadric surfaces has been determined. Angular bounds determined theoretically have been proved experimentally for all of the quadric surfaces.

The equations of the planes which determine distinct feature vectors for each of the quadric surfaces are very sensitive to the quality of the digitized range data. In case the coefficient determining algorithm does not perform as expected, errors might be encountered while forming the feature sets. Active sensors like laser range mappers have only recently been developed. Much improvement is expected in the quality of range images in the near future. This will make the various recognition schemes much more reliable and flexible.

The successful performance of the segmentation scheme would enable to extend our recognition system to recognize irregular surfaces which are made up piece-by-piece of regular quadric surfaces.

Appendix 1

Formulation of the Rotational Matrix and Determination of the New Quadric Coefficients

Let (x,y,z) describe the coordinates of any point (Figure (a1)) in our coordinate system. As shown in Figure (a2), consider a rotation of angle α about the z axis, i.e. in the xy -plane. Then the new coordinates in terms of the old are represented as

$$x = x'\cos\alpha + y'\sin\alpha$$

and

$$y = -x'\sin\alpha + y'\cos\alpha;$$

i.e., the rotation matrix is

$$R_\alpha = \begin{bmatrix} \cos\alpha & \sin\alpha & 0 \\ -\sin\alpha & \cos\alpha & 0 \\ 0 & 0 & 1 \end{bmatrix}.$$

Next, as shown in Figure (a3), consider a rotation about the x' axis by an angle β , i.e., in the $y'z$ plane, of the same point. The resultant coordinates and the old coordinates are now related by the following equations:

$$y' = y''\cos\beta + z'\sin\beta$$

and

$$z = -y''\sin\beta + z'\cos\beta,$$

where the rotation matrix is

$$R_\beta = \begin{bmatrix} 1 & 0 & 0 \\ 0 & \cos\beta & \sin\beta \\ 0 & -\sin\beta & \cos\beta \end{bmatrix}.$$

Finally as shown in Figure (a4), consider a rotation about the y'' axis by an angle γ , i.e., in the $x'z'$ plane, then

$$z' = z''\cos\gamma + x''\sin\gamma$$

and

$$x' = -z''\sin\gamma + x''\cos\gamma.$$

The rotation matrix for the above transformation is

$$R_\gamma = \begin{bmatrix} \cos\gamma & 0 & -\sin\gamma \\ 0 & 1 & 0 \\ \sin\gamma & 0 & \cos\gamma \end{bmatrix}.$$

Observing that

$$\begin{bmatrix} x \\ y \\ z \end{bmatrix} = R_\alpha R_\beta R_\gamma \begin{bmatrix} x'' \\ y'' \\ z'' \end{bmatrix},$$

we obtain the following:

$$x = x''(\cos\alpha\cos\gamma + \sin\alpha\sin\beta\sin\gamma) + y''\sin\alpha\cos\beta + z''(-\sin\gamma\cos\alpha + \cos\gamma\sin\alpha\sin\beta),$$

$$y = x''(-\cos\gamma\sin\alpha + \sin\gamma\sin\beta\cos\alpha) + y''\cos\beta\cos\alpha + z''(\sin\gamma\sin\alpha + \cos\gamma\sin\beta\cos\alpha)$$

and

$$z = x''\sin\gamma\cos\beta - y''\sin\beta + z''\cos\gamma\cos\beta.$$

After substituting the new x , y , and z coordinates into Equation (1) (Section 3), we get an entire set of new coefficients for x''^2 , y''^2 , z''^2 , $y''z''$, $x''z''$, $x''y''$, x'' , y'' , and z'' .

These new coefficients are as follows:

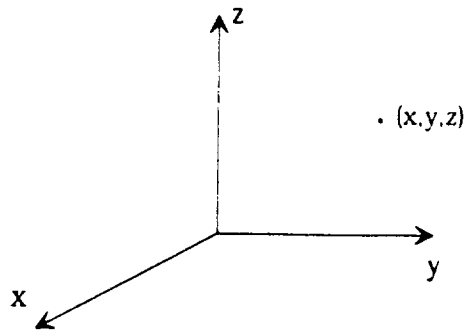


Figure (a1)

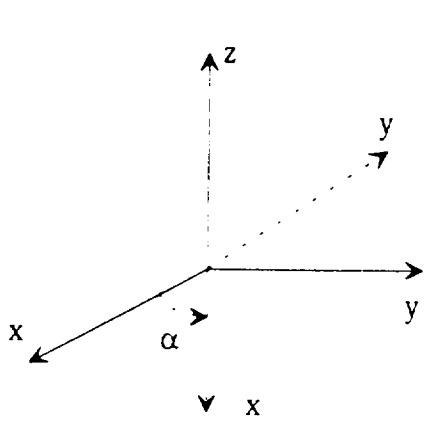


Figure (a2)

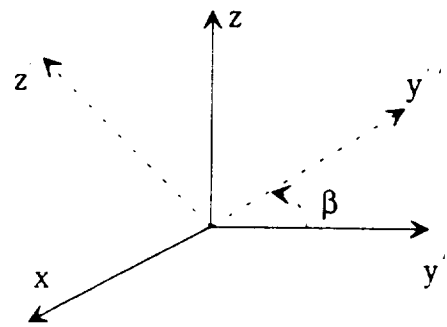


Figure (a3)

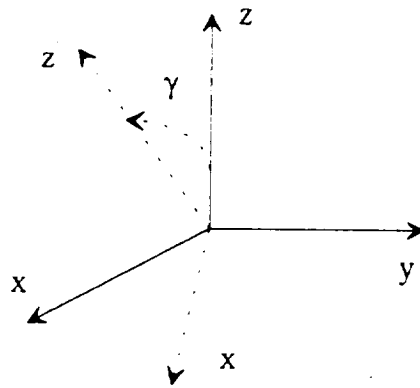


Figure (a4)

$$\begin{aligned}
a'' &= \cos^2\gamma [a \cdot \cos^2\alpha + b \cdot \sin^2\alpha] + \sin^2\beta \sin^2\gamma [a \cdot \sin^2\alpha + b \cdot \cos^2\alpha] \\
&+ 2\sin\alpha \sin\beta \sin\gamma \cos\alpha \cos\gamma (a - b) + c \cdot \sin^2\gamma \cos^2\beta \\
&+ \sin 2\alpha [h \cdot \sin^2\beta \sin^2\gamma] + \sin 2\gamma [-f \cdot \sin\alpha \cos\beta + g \cdot \cos\alpha \cos\beta \\
&+ h \cdot \cos^2\alpha \sin\beta - h \cdot \sin\beta \sin^2\alpha] + \sin 2\beta \sin^2\gamma (f \cdot \cos\alpha + g \cdot \sin\alpha) - h \cdot \sin 2\alpha \cos^2\gamma.
\end{aligned}$$

$$\begin{aligned}
b'' &= (a \cdot \sin^2\alpha + b \cdot \cos^2\alpha) \cos^2\beta + c \cdot \sin^2\beta + \sin 2\beta [-f \cdot \cos\alpha - g \cdot \sin\alpha] \\
&+ h \cdot \sin 2\alpha \cos^2\beta.
\end{aligned}$$

$$\begin{aligned}
c'' &= \sin^2\gamma (a \cdot \cos^2\alpha + b \cdot \sin^2\alpha) + (a \cdot \sin^2\alpha + b \cdot \cos^2\alpha) \cos^2\gamma \sin^2\beta \\
&+ 2\sin\alpha \sin\beta \sin\gamma \cos\alpha \cos\gamma (b - a) + c \cdot \cos^2\gamma \cos^2\beta + \sin 2\alpha [h \cdot \cos^2\gamma \sin^2\beta - h \cdot \sin^2\gamma] \\
&+ \cos^2\gamma \sin 2\beta [f \cdot \cos\alpha + g \cdot \sin\alpha] + \sin 2\gamma [f \cdot \sin\alpha \cos\beta - g \cdot \cos\alpha \cos\beta - h \cdot \cos 2\alpha \sin\beta].
\end{aligned}$$

$$\begin{aligned}
2f'' &= \left[(b \cdot \cos^2\alpha + a \cdot \sin^2\alpha + h \cdot \sin 2\alpha - c) \sin 2\beta + (2g \cdot \sin\alpha + 2f \cdot \cos\alpha) \cos 2\beta \right] \cos\gamma \\
&+ \left[((b - a) \sin 2\alpha - 2h \cdot \cos 2\alpha) \cos\beta + (2g \cdot \cos\alpha - 2f \cdot \sin\alpha) \sin\beta \right] \sin\gamma.
\end{aligned}$$

$$\begin{aligned}
2g'' &= \sin 2\gamma \left[-\cos^2\alpha (a - b \cdot \sin^2\beta) - \sin^2\alpha (-a \cdot \sin^2\beta + b) + c \cdot \cos^2\beta \right] \\
&+ \sin 2\gamma \left[\sin 2\beta (f \cdot \cos\alpha + g \cdot \sin\alpha) + h \cdot \sin 2\alpha (1 + \sin^2\beta) \right] \\
&+ \cos 2\gamma \left[\sin 2\alpha \sin\beta (a - b) + 2h \cdot \sin\beta \cos 2\alpha + \cos\beta (2g \cdot \cos\alpha - 2f \cdot \sin\alpha) \right].
\end{aligned}$$

$$\begin{aligned}
2h'' &= \sin 2\beta \sin\gamma [a \cdot \sin^2\alpha + b \cdot \cos^2\alpha - c + h \cdot \sin 2\alpha] + \cos 2\beta \sin\gamma [2g \cdot \sin\alpha + 2f \cdot \cos\alpha] \\
&+ \cos\beta \cos\gamma [\sin 2\alpha (a - b) + 2h \cdot \cos 2\alpha] + \sin\beta \cos\gamma [2f \cdot \sin\alpha - 2g \cdot \cos\alpha].
\end{aligned}$$

$$2p'' = 2\cos\gamma [p \cdot \cos\alpha - q \cdot \sin\alpha] + 2\sin\beta \sin\gamma [p \cdot \sin\alpha + q \cdot \cos\alpha] + 2r \cdot \sin\gamma \cos\beta.$$

$$2q'' = 2\cos\beta [p \cdot \sin\alpha + q \cdot \cos\alpha] - 2r \cdot \sin\beta.$$

$$2r'' = 2\cos\gamma \sin\beta [p \cdot \sin\alpha + q \cdot \cos\alpha] + 2\sin\gamma [-p \cdot \cos\alpha + q \cdot \sin\alpha] + 2r \cdot \cos\gamma \cos\beta.$$

$$d'' = d.$$

We are now in a position to formulate a rotation matrix whose elements correspond to the directional cosines of the x, y, and z axes of the rotated object.

The rotation matrix = $R_\gamma R_\beta R_\alpha$,

where

$$R_{\alpha} = \begin{bmatrix} \cos\alpha & \sin\alpha & 0 \\ -\sin\alpha & \cos\alpha & 0 \\ 0 & 0 & 1 \end{bmatrix},$$

$$R_{\beta} = \begin{bmatrix} 1 & 0 & 0 \\ 0 & \cos\beta & \sin\beta \\ 0 & -\sin\beta & \cos\beta \end{bmatrix},$$

and

$$R_{\gamma} = \begin{bmatrix} \cos\gamma & 0 & -\sin\gamma \\ 0 & 1 & 0 \\ \sin\gamma & 0 & \cos\gamma \end{bmatrix}.$$

Subsequently,

$$R_{\gamma}R_{\beta}R_{\alpha} = \begin{bmatrix} \cos\alpha\cos\gamma - \sin\alpha\sin\beta\sin\gamma & \cos\gamma\sin\alpha + \sin\gamma\sin\beta\cos\alpha & -\sin\gamma\cos\beta \\ -\cos\beta\sin\alpha & \cos\beta\cos\alpha & \sin\beta \\ \sin\gamma\cos\alpha + \cos\gamma\sin\alpha\sin\beta & \sin\alpha\sin\gamma - \cos\gamma\sin\beta\cos\alpha & \cos\beta\cos\gamma \end{bmatrix},$$

where

$$\alpha = \sum_{i=1}^n \alpha_i, \quad \beta = \sum_{i=1}^n \beta_i, \quad \text{and} \quad \gamma = \sum_{i=1}^n \gamma_i. \quad n \text{ corresponds to the iteration where all the rota-}$$

tion terms go to zero in the limit.

REFERENCES

- [1] P. J. Besl and R. C. Jain, "Three-Dimensional Object Recognition," *ACM Comput. Surveys*, vol 17, pp. 77-145, March 1985.
- [2] R. A. Jarvis, "A Perspective on Range Finding Techniques for Computer Vision," *IEEE Trans. on Pattern Analysis and Machine Intelligence*, PAMI-5, pp. 122-139, March 1983.
- [3] M. Ishii and T. Nagata, "Feature Extraction of Three-Dimensional Objects and Visual Processing in a Hand-Eye System using Laser Tracker," *Pattern Recognition* vol. 8, pp. 229-237, 1976.
- [4] O. D. Faugeras et.al, "Towards a Flexible Vision System," *Robot Vision*, U.K., 1982.
- [5] M. Oshima and Y. Shirai, "Object Recognition using Three-Dimensional information," *IEEE Trans. on Pattern Analysis and Machine Intelligence*, PAMI-5, No. 4, pp. 353-361, July 1983.
- [6] B. Bhanu, "Representation and Shape Matching of 3-D Objects," *IEEE Trans. on Pattern Analysis and Machine Intelligence* , PAMI-6, No. 3, pp. 340-350, 1984.
- [7] R. Nevatia and T. O. Binford, "Description and Recognition of Curved Objects," *Artificial Intelligence*, 8, pp. 77-98, 1977.
- [8] I. K. Sethi and S. N. Jayaramamurthy, "Surface Classification using Characteristic Contours," Proc. 7th Intl. Conf. on Pattern Recognition, Montreal-Canada, pp. 438-440, 1984.
- [9] P. J. Besl and R. C. Jain, "Invariant Surface Characteristics for 3D Object Recognition in Range Images," *IEEE Trans. on Computer Vision, Graphics and Image Processing*, 33, 1, pp. 33-80, January 1986.

- [10] N. Alvertos and I. D’Cunha, "Three-Dimensional Description of Symmetric Objects from Range Images," SPIE vol 1382, Intelligent Robots and Computer Vision IX: Neural, Biological, and 3-D Methods, pp. 388-396, 1990.
- [11] N. Yokoya and M. D. Levine, "Range Image Segmentation based on Differential Geometry: A Hybrid Approach," McRCIM-TR-CIM 87-16, 1987.
- [12] W. E. L. Grimson and T. Lozano-Perez, "Model Based Recognition and Localization from Sparse Range data," *Techniques for 3-D Machine perception*, Elsevier Science Publishers (North Holland), pp. 113-148, 1986.
- [13] O. D. Faugeras and M. Hebert, "The Representation, Recognition, and Positioning of 3-D Shapes from Range Data," *Techniques for 3-D Machine Perception*, Elsevier Science Publishers (North Holland), 1986.
- [14] G. Hu and G. Stockman, "3-D Surface Solution using Structured Light and Constraint Propagation," *IEEE Trans. on Pattern Analysis and Machine Intelligence*, vol. 11, No. 4, April 1989.
- [15] M. Nagao, S. Hashimoto, and T. Saka, *Automatic Model Generation and Recognition of Simple Three-Dimensional Bodies*, " New York: Academic Press, Inc., 1973.
- [16] S. Ullman and R. Basri, "Recognition by Linear Combination of Models," *IEEE Trans. on Pattern Analysis and Machine Intelligence*, vol. 13, No. 10, pp. 992-1006, October 1991.
- [17] T. J. Fan, G. Medioni, and R. Nevatia, "Recognizing 3-D Objects using Surface Descriptors," *IEEE Trans. on Pattern Analysis and Machine Intelligence*, vol. 11, No. 11, pp. 1140-1157, November 1989.
- [18] D. Forsyth, J. L. Mundy, A. Zisserman, C. Coelho, A. Heller, and C. Rothwell, "Invariant Descriptors for 3-D Object Recognition and Pose," *IEEE Trans. on Pattern Analysis and Machine Intelligence*, vol. 13, No. 10, pp. 971-991, October

1991.

- [19] S. Lee and H. Hahn, "An Optimal Sensing Strategy for Recognition and Localization of 3-D Natural Quadric Objects," *IEEE Trans. on Pattern Analysis and Machine Intelligence*, vol. 13, No. 10, pp. 1018-1037, October 1992.
- [20] N. C. Grisworld and C. P. Yeh, "A New Stereo Vision Model Based upon the Binocular Fusion Concept," *IEEE Trans. on Computer Vision, Graphics, and Image Processing*, 41, pp. 153-171, 1988.
- [21] D. Marr and T. Poggio, "A Computational Theory of Human Stereo Vision," *Proc. R. Soc. London, B* 204, pp. 301-308, 1979.
- [22] W. E. L. Grimson, "Computational Experiments with Feature Based Stereo Algorithms," *IEEE Trans. on Pattern Analysis and Machine Intelligence*, PAMI-7, pp. 17-34, 1985.
- [23] R. P. Wilder, "Qualitative Three-Dimensional Shape from Stereo," *Proc. SPIE, Intelligent Robots and Computer Vision IX: Neural, Biological, and 3-D Methods*, vol 13382, pp. 453-463, 1990.
- [24] N. Alvertos and I. D'Cunha, "Curvature Effect of Median Filtering on Range Images," *IEEE proc. of Southeastcon 1991*, vol. 2, pp. 910- 914, 1991.
- [25] B. Groshong and G. Bilbro, "Fitting a Quadric Surface to Three-Dimensional Data," technical Report, January 1986.
- [26] J. M. H. Olmstead, *Solid Analytical Geometry*. New York: Appleton-Century-Crofts. Inc., 1947.
- [27] Digital Signal Corporation, *Laser Radar 3-D Vision System Operation Manual*, contract no. NAS-18522, October 1988.
- [28] B. Sabata, F Arman, J. K. Aggarwal, "Segmentation of 3D Range images using Pyramidal Data structures," *CVGIP: Image Understanding*, Vol. 57, No. 3, May 1993, pp. 373-387.

[29] T. Pavlidis, *Algorithms for Graphics and Image Processing*, Rockville, MD., Computer Science Press, 1982.

[30] I. D'Cunha, *Optical Machine Recognition of Lower-Case Greek Characters of Any Size*, M.S. Thesis, Old Dominion University, 1989.